Geophys. J. Int. (2007) **169,** 1229–1238 doi: 10.1111/j.1365-246X.2007.03375.x

Far-field simulation of the 1946 Aleutian tsunami

Emile A. Okal[1] and Hélène Hébert[2]

[1] *Department of Geological Sciences, Northwestern University, Evanston,* IL 60201, *USA. E-mail: emile@earth.northwestern.edu*
[2] *Département Analyse et Surveillance de l'Environnement, Commissariat à l'Energie Atomique, Boîte Postale* 12, 91680 *Bruyères-le-Châtel, France*

Accepted 2007 January 30. Received 2007 January 30; in original form 2006 July 8

SUMMARY

We present hydrodynamic far-field simulations of the Aleutian tsunami of 1946 April 1, using both a dislocation source representing a slow earthquake and a dipolar one modelling a large landslide. The earthquake source is derived from the recent seismological study by López and Okal, while the landslide source was previously used to explain the exceptional run-up at Scotch Cap in the near field. The simulations are compared to a field data set previously compiled from testimonies of elderly witnesses at 27 far-field locations principally in the Austral and Marquesas Islands, with additional sites at Pitcairn, Easter and Juan Fernández. We find that the data set is modelled satisfactorily by the dislocation source, while the landslide fails to match the measured amplitudes, and to give a proper rendition of the physical interaction of the wavefield with the shore, in particular at Nuku Hiva, Marquesas. The emerging picture is that the event involved both a very slow earthquake, responsible for the far-field tsunami, and a major landslide explaining the near-field run-up, but with a negligible contribution in the far field.

Key words 1946 Aleutian earthquake, Tsunami earthquake, Tsunami simulation.

1 INTRODUCTION AND BACKGROUND

This paper presents hydrodynamic simulations in the far field of the tsunami generated by the Aleutian earthquake of 1946 April 1 (Fig. 1). This event remains a challenge to geophysicists, as it generated a much larger tsunami than expected from its conventional magnitude, $M = 7.4$ as measured at Pasadena and reported by Gutenberg & Richter (1954). In the near field, the tsunami eradicated the lighthouse at Scotch Cap on Unimak Island (Sanford 1946), where recent field work (Okal *et al.* 2003) has mapped run-up to an elevation of 42 m. In the far field, the tsunami wrought considerable damage in the Hawaiian Islands (where it killed 159 persons), the Marquesas Islands, Easter and even reportedly at Winter Island on the shores of Antarctica (Fuchs 1982). This discrepancy between tsunami amplitude and earthquake magnitude was investigated by Kanamori (1972) who included the Aleutian event as a charter member of the class of so-called 'tsunami earthquakes', whose tsunamis are larger than suggested by their magnitudes, especially those measured using conventional algorithms. Such disparities have generally been ascribed to exceedingly slow rupture velocities along the seismic fault, which leads to destructive interference for all seismic waves in the most commonly registered frequency bands, and thus to a systematic underestimation of the true size of the seismic source. Indeed, a recent seismological investigation of the 1946 event reveals a very slow bilateral rupture with a static moment of 8.5×10^{28} dyn-cm, ranking it among the ten largest earthquakes ever recorded (López & Okal 2006).

On the other hand, in the wake of the 1998 Papua New Guinea tsunami, which killed more than 2200 people in the near field, it was realized that underwater landslides could be unsuspected but major contributors to the generation of near-field tsunamis (Synolakis *et al.* 2002), and thus the question naturally arose of the possible contribution of a landslide to the source of the 1946 Aleutian tsunami. This possibility was mentioned early on by Macdonald *et al.* (1947), who discounted it on the basis of a qualitative discussion of the properties of the tsunami in the far field, and later by Kanamori (1985). The existence of a landslide as a component to the source of the 1946 Aleutian tsunami was proposed again by Okal *et al.*'s (2003) simulation of the data set of near-field run-up measurements collected by these authors on Unimak and Sanak Islands. In lay terms, they argued that the excessive run-up at and near Scotch Cap (up to 42 m) could not be reconciled with the seismic slip of even a gigantic earthquake, in illustration of simple scaling laws for tsunamis in the near field, as later investigated systematically by Okal & Synolakis (2004). Rather, Okal *et al.* (2003) showed that the near-field run-up could be modelled satisfactorily using a dipolar source representing a 200-km^3 landslide which will be described in greater detail in Section 3. The occurrence of a landslide was also suggested by anecdotal reports from elderly fishermen and by qualitative disparities between bathymetric charts pre- and post-dating the event (Okal *et al.* 2003). More recently, Fryer *et al.* (2004) have proposed that the whole 1946 event consisted of a major landslide, without a *bona fide* seismic dislocation, a model difficult to reconcile with the spatial and temporal distribution of aftershocks (López & Okal 2006).

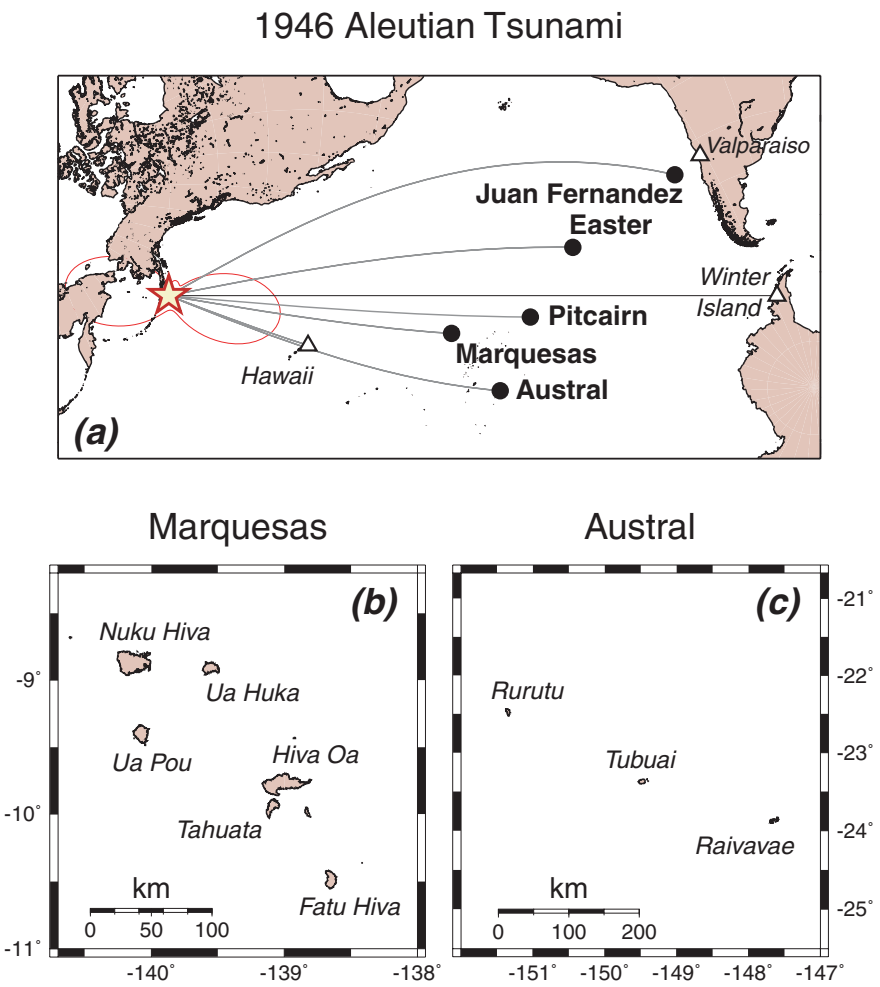

Figure 1. (a) Location map of the source of the 1946 Aleutian earthquake (star) and of the island groups considered in this study (solid dots). This is an oblique Mercator projection using the great circle from Unimak to Winter Island as its baseline (Equator); as such, it is conformal, and gives an appropriate representation of the directivity of the tsunami at the source, shown as the bow-tie azimuthal pattern surrounding the epicentre. (b) and (c) Close up maps of the Polynesian island groups; these are standard Mercator projections.

On the other hand, Johnson & Satake (1997) used dislocation sources to model a number of tidal gauge records of the tsunami in the far field, suggesting a moment of 2.3×10^{28} dyn-cm, but failed to obtain a satisfactory fit for the largest amplitudes, namely at Honolulu. Finally, Tanioka & Seno (2001) invoked the possible influence of splay faults in the accretionary prism, an idea first expressed by Fukao (1979), to reconcile far-field tidal gauge records, including the one at Honolulu, with a relatively weak seismic source. However, their proposed seismic moment (1.8×10^{28} dyn-cm) remains much smaller than modelled by López & Okal (2006), reflecting a much narrower fault zone, incompatible with these authors' reassessment of the aftershock distribution.

In this context, the present study offers a series of transpacific hydrodynamic simulations of the 1946 Aleutian tsunami in the far field, using as initial conditions both López & Okal's (2006) dislocation source, and the dipolar source introduced by Okal *et al.* (2003) to model the tsunami in the near field. By comparing our results with the data set of far-field run-up values gathered by Okal *et al.* (2002), we conclude that the far-field tsunami is well modelled by the dislocation source.

2 THE DISLOCATION SOURCE

The dislocation source used in the present study is based on the recent seismological model by López & Okal (2006), obtained from the modelling of the spectra of low-frequency mantle waves, and the relocation of a full set of 39 aftershocks. It features a bilateral rupture propagating 80 km northeast and 120 km southwest along the Pacific-North American Plate boundary, as defined by the Aleutian trench, striking N63°E. López & Okal (2006) have proposed a very slow velocity of rupture, $V_R = 1.12$ km s^{-1}, which, combined with the bilateral character of the source, results in destructive interference for all seismic waves in all azimuths even at frequencies characteristic of mantle waves. However, V_R remains hypersonic with respect to all tsunami phase velocities C (typically 220 m s^{-1} in the deep ocean) and thus, following Ben-Menahem & Rosenman (1972), constructive interference is expected for the far-field tsunami in the azimuth perpendicular to the rupture.

Based on López & Okal's (2006) moment of $M_0 = 8.5 \times 10^{28}$ dyn-cm, and on the dimensions of the fault revealed by the distribution of aftershocks (length $L = 200$ km; width $W = 120$ km), we use a

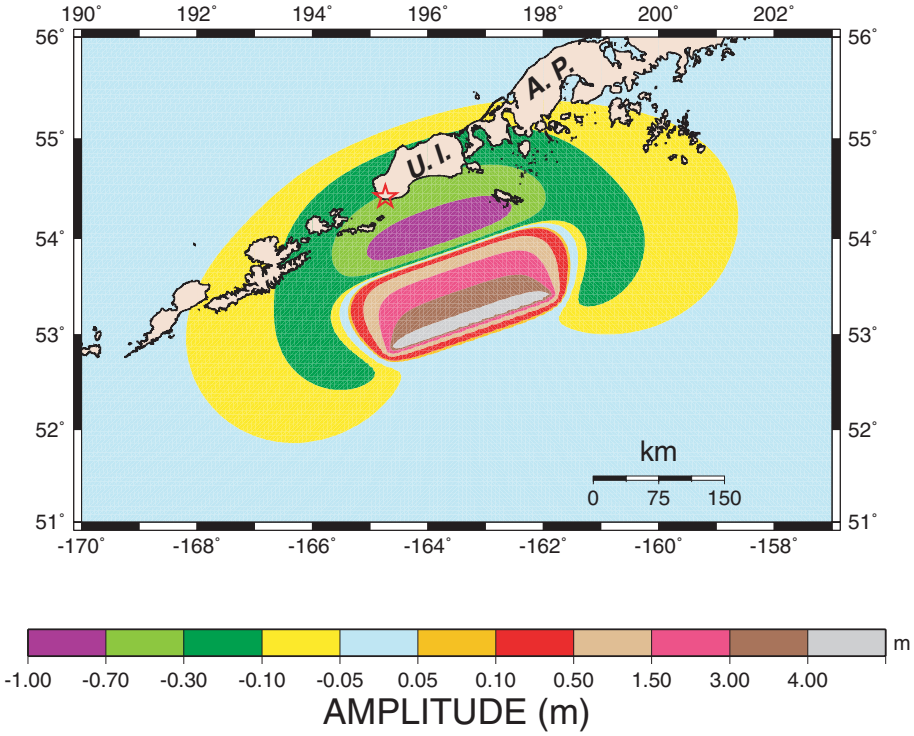

Figure 2. Static displacement field computed for the dislocation source, and taken as the initial condition of the simulation. The coastlines of the Alaskan Peninsula (A.P.) and of the adjoining islands, including Unimak (U.I.) are superimposed. The star identifies Scotch Cap, site of the lighthouse eradicated by the tsunami.

slip $\Delta u = 9$ m. The focal geometry ($\phi = 243°$; $\delta = 10°$; $\lambda = 90°$) used by López & Okal (2006) was derived by Pelayo (1990) from body-wave modelling. We then derived the static field of vertical displacement in the source region by implementing the algorithm of Mansinha & Smylie (1971). In turn, these values were used as initial conditions for the vertical deformation of the ocean surface, $\eta(x, y; t = 0_+)$. This assumption, widely used in numerical simulation of ocean wide tsunamis, is legitimate in view of the high value of the ratio $V_R/C \approx 5$, which allows to consider the whole seismic rupture as an instantaneous source of the tsunami. To complement the initial conditions, we take zero horizontal flow averaged over the ocean column: $U(x, y; t = 0_+) = V(x, y; t = 0_+) = 0$. Fig. 2 shows the distribution of initial values of η in the vicinity of the source. The maximum value of η is 5.23 m; the minimum corresponds to a subsidence of 97 cm.

3 THE DIPOLAR SOURCE

The dipolar source used in this study models the initial field due to a large landslide featuring a volume of 200 km^3 moving at an average speed of ~30 m s^{-1} along the continental slope off Davidson Bank. As discussed by Okal & Synolakis (2004), the initial surface displacement takes the form of a dipolar function featuring a negative trough and a positive hump separated by a 35-km lever oriented N165°E, that is, along the line of steepest slope. The distribution of subsidence in the trough is taken as

$$\eta(x, y) = \eta_- \cdot \left(\mathrm{sech}\frac{4X}{W_X}\right)^2 \cdot \left(\mathrm{sech}\frac{4Y}{W_Y}\right)^2, \qquad (1)$$

where $\eta_- = -28$ m, Y is the geographic coordinate in the azimuth of steepest slope ($\phi = 165°$), X the coordinate perpendicular to Y, and the transverse dimensions of the trough are $W_X = 52.5$ km; $W_Y = 35$ km. The positive hump obeys a similar distribution, but with values of W increased by a factor 1.21, and a maximum height reduced by the same factor, squared ($\eta_+ = 19$ m), so that the total integral of displaced water at the surface is zero; it is activated 1000 s later than the trough, to express the slow evolution of the landslide on the ocean floor. This model, which treats the source as two instantaneous, if time-lagged, impulses, is clearly an oversimplification, as it ignores the complex phenomenon of a large landslide, which may in particular evolve into a turbidity current. However, this source was used successfully by Okal *et al.* (2003) to model the exceptional near-field run-up of 42 m at Scotch Cap. A similar but smaller source was used to model the 1998 Papua New Guinea tsunami in the near field (Heinrich *et al.* 2000; Synolakis *et al.* 2002). Fig. 3 shows the distribution of initial values of η in the source area. A comparison between Figs 2 and 3 underscores the fundamental difference between the two sources, the field of initial displacement of the dipolar source being both of much larger amplitude and spatially more concentrated than its dislocation counterpart.

4 THE RUN-UP DATA SET

We model the data set obtained by Okal *et al.* (2002), based on the interview of elderly witnesses of the 1946 tsunami at transpacific sites, including the Marquesas, Easter and Juan Fernández Islands (Fig. 1). Fig. 4(a), from Okal *et al.* (2002), summarizes the product of this survey in the case of Nuku Hiva, the northernmost main island of the Marquesas group. We elect not to model those sites involving riverbeds, with run-up values shown in italics on the figure, as the value of the run-up is more strongly influenced by the local topography.

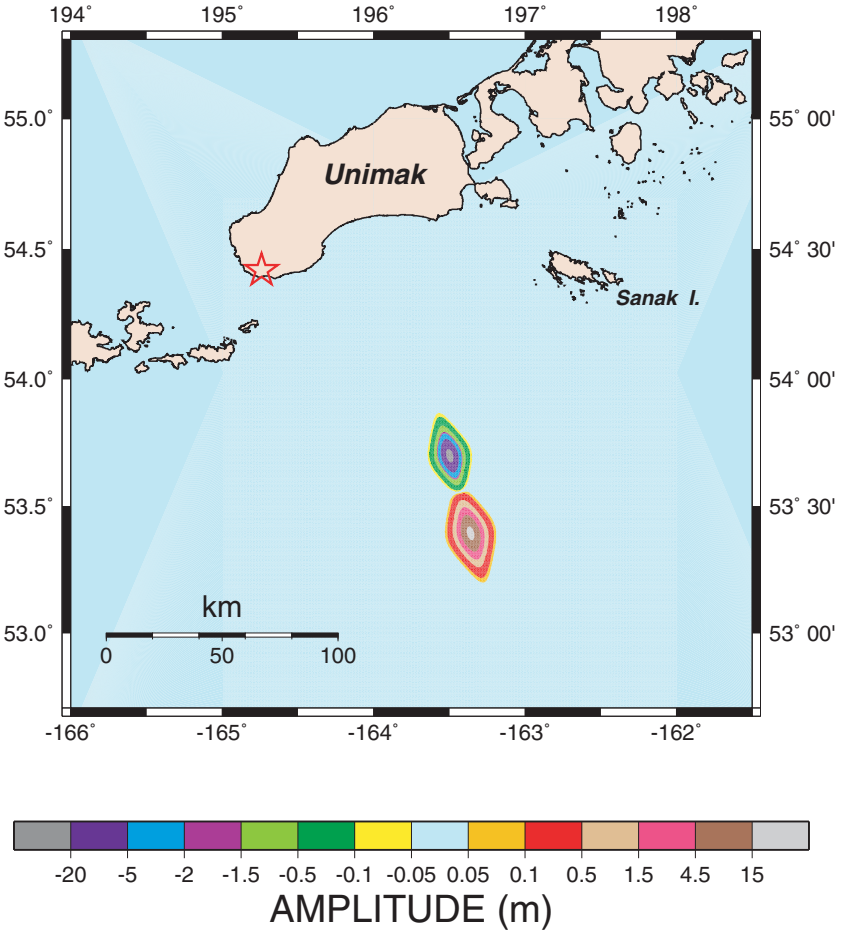

Figure 3. Static displacement field computed for the landslide source, and taken as the initial condition of the simulation. Note the difference in scale with Fig. 2, and the use of a different color palette, expressing the larger amplitudes and the greater spatial concentration of the source.

We supplement this data set with similar measurements taken in 2001 December and 2002 March on the Austral Islands (Tubuai, Rurutu and Raivavae) and in 2003 at Pitcairn Island, as shown on Figs 4(b–e), which complement the individual island plots published by Okal *et al.* (2003). Note that strong run-up values, reaching 5–6 m, are found on Pitcairn and Rurutu, which lack a substantial coral reef system, the former because of its youth (Duncan *et al.* 1974), the latter as a result of its complex history of tectonic uplift (Chauvel *et al.* 1997), such values being generally comparable to the results in the Marquesas. By contrast, Tubuai and Raivavae, ringed by reef systems reaching a width of 3–5 km, feature more moderate values of run-up, not exceeding 3 m. Finally, we do not consider those sites for which no detailed bathymetry is readily available on the scale of the individual bay [e.g. Anahou (Nuku Hiva) or Hauti (Rurutu)].

The resulting data set, consisting of 27 run-up values, is listed in Table 1, in which island groups are arranged from west to east and numbers in brackets refer to, and complement, the individual sites in Okal *et al.*'s (2002) survey.

5 THE SIMULATION

5.1 Methodology

For each of the possible sources, we proceed to carry out a full simulation of the propagation of the tsunami across the Pacific Ocean, of its interaction with the relevant islands, and of the run-up at the sites listed in Table 1. The simulation uses a finite difference code, introduced by Guibourg *et al.* (1997), which solves the equation of hydrodynamics under the non-linear Shallow Water Approximation. In the present applications, we neglect the effect of friction at the bottom of the ocean, as well as Coriolis terms.

The computation follows the algorithm of Hébert *et al.* (2001). It is performed on a set of successively refined grids involving five different levels of spatial and time steps. All gridding is done at regular intervals of latitude and longitude, and thus involves a correction of the equations of hydrodynamics for Earth sphericity. At the basin level on the high seas, we use a first grid with a spatial step of 6 min of arc (0.1 degree or ∼11 km in latitude), and a time step of 8 s. The bathymetry is obtained by decimating Smith & Sandwell's (1997) data set. At the level of an island group (typically over a linear distance of 300 km, and at depths shallower than 3000 m), we use a second grid with a spatial step of 1 min of arc (1 nautical mile or ∼1.8 km in latitude), and a time step of 2 s. The gridding is further refined at a third level (10 s of arc or ∼300 m in latitude and 0.5 s in time) at the scale of an individual island and at a fourth level (2 s of arc or ∼60 m in latitude and 0.25 s in time) at the scale of an individual bay. Finally, the inundation of initially dry land is calculated using a fifth grid with a spatial resolution of 0.5 s of arc (∼15 m in latitude) and 0.125 s in time. The time steps used are matched to the individual spatial grids in order to

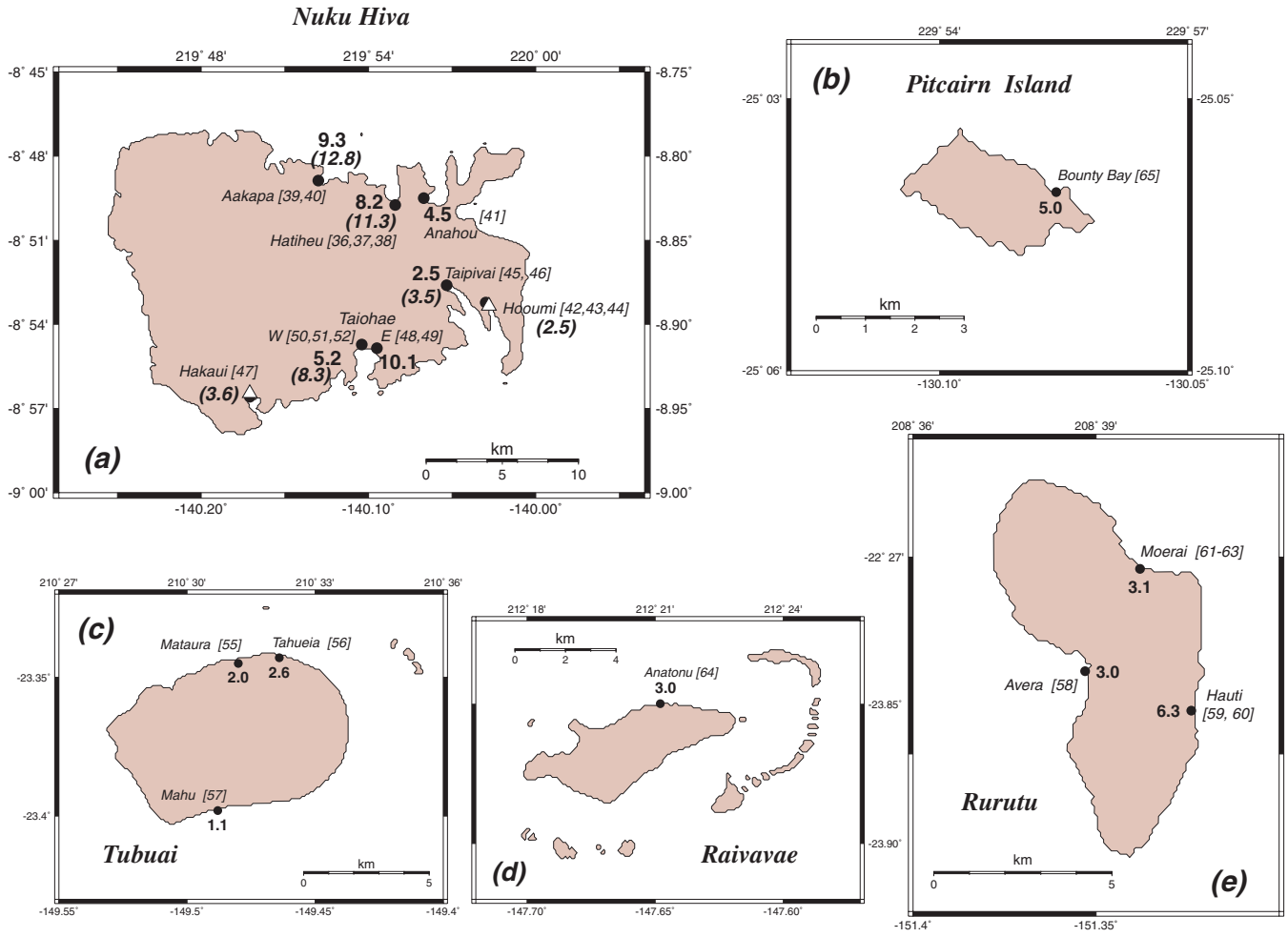

Figure 4. (a) Example of summary of field survey results on the island of Nuku Hiva (Marquesas), after Okal *et al.* (2002). At each location, the bold number indicates the largest surveyed run-up (in metres) at overland sites and the numbers in bold italics (in parentheses) those measured in riverbeds (not used in the present study). The numbers in brackets are the site numbers listed in Okal *et al.* (2002). The open triangles show locations where large coral blocks were moved inland by the 1946 tsunami. (b) Field survey results at Pitcairn Island. (c) Field survey results at Tubuai (Austral Islands). (d) Field survey results at Raivavae (Austral Islands). (e) Field survey results at Rurutu (Austral Islands).

comply with the Courant-Friedrichs-Lewy (CFL) condition for numerical stability (Courant *et al.* 1928); they decrease slower than the spatial grid steps, reflecting the lesser velocities of the wave in shallower waters. Detailed bathymetric information (as well as relevant topographic data for run-up calculations) was hand-digitized and interpolated from a variety of nautical charts obtained principally from the British Admiralty series and the French Navy's *Service Hydrographique et Océanographique de la Marine*. The exact locations at which the transitions from one level of gridding to the next took place were site dependent.

In the case of the dipolar source, the initial evolution of the wavefield in the source area was computed using only the negative trough on an auxiliary grid featuring a spatial step of 0.01 degree (∼1.1 km in latitude) and a time step of 1 s; the positive hump is switched on after a delay of 1000 s, and the computation continued for 300 s, and then transferred to a second grid with a spatial step of 1 min of arc (∼1.8 km in latitude) and a time step of 4 s, which runs for 10 000 s (∼2.8 hr), before being transferred to the coarsest transoceanic grid described above. This procedure is necessary to provide stability to a wavefield dominated by much shorter wavelengths than in the case of the dislocation source.

5.2 Results

The results of our simulations can be expressed in a number of ways.

(1) *Run-up values.* First, we consider maps of maximum wave heights (at sea) or run-up (on originally dry land) for a time window extending at least 2 hr after the group arrival time of the tsunami. Fig. 5 gives an example in the case of Puamau (Site *[11]*) on the island of Hiva Oa (Marquesas). The datum reported by Okal *et al.* (2002) consisted of a run-up value ($M = 6.5$ m) at the location of the arrow on Fig. 5. Our maps indicate simulated values $D = 5.5$ m and $L = 2.4$ m, for the dislocation and landslide sources, respectively.

Table 1 and Fig. 6 compile the final results of our simulated run-up computations at all 27 overland locations in the far field, both in the case of the dislocation (earthquake) and dipolar (landslide) sources, and compare them to the surveyed data set. It is immediately clear that the earthquake source fits the observations better than the landslide one. The quality of this fit can be quantified by defining, for each location, a logarithmic residual r

$$r = \log_{10} \frac{\eta_{Simulated}}{\eta_{Observed}} \qquad (2)$$

Table 1. Data set of measured and simulated run-up values.

Site	Island	Reference number	Simulated run-up (m)			Ratios	
			Measured run-up (m) M	Dislocation, D	Landslide, L	D/M	L/M
Austral Islands							
Mataura	Tubuai	*[55]*	2.0	2.0	1.1	1.00	0.55
Tahueia	Tubuai	*[56]*	2.6	1.5	1.0	0.58	0.38
Avera	Rurutu	*[58]*	3.0	2.5	0.3	0.87	0.10
Moerai	Rurutu	*[63]*	3.1	2.5	0.5	0.81	0.16
Anatonu	Raivavae	*[64]*	3.0	3.0	1.3	1.00	0.43
Marquesas Islands							
Omoa	Fatu Hiva	*[1]*	2.5	4.0	1.0	1.60	0.40
Hanavave	Fatu Hiva	*[2]*	6.0	5.5	1.9	0.92	0.32
Hanamenu	Hiva Oa	*[4]*	7.5	6.0	2.0	0.80	0.27
Hanaiapa	Hiva Oa	*[5]*	5.9	5.0	1.4	0.85	0.24
Hanaiapa	Hiva Oa	*[7]*	10.4	5.5	2.1	0.53	0.20
Hanatekuua	Hiva Oa	*[8]*	6.6	6.0	2.1	0.91	0.32
Puamau	Hiva Oa	*[11]*	6.5	5.5	2.4	0.85	0.37
Taaoa	Hiva Oa	*[14]*	5.6	3.5	0.9	0.63	0.16
Vaitahu	Tahuata	*[19]*	7.3	5.3	1.3	0.73	0.18
Hapatoni	Tahuata	*[21]*	4.0	3.2	0.8	0.80	0.20
Hakahetau	Ua Pou	*[23]*	6.1	4.5	1.7	0.74	0.28
Hakahau	Ua Pou	*[28]*	7.2	5.0	1.4	0.69	0.19
Hakatao	Ua Pou	*[30]*	5.8	3.5	2.0	0.60	0.34
Hokatu	Ua Huka	*[34]*	3.2	2.5	1.3	0.78	0.41
Hatiheu	Nuku Hiva	*[38]*	8.2	7.0	1.8	0.85	0.22
Aakapa	Nuku Hiva	*[39]*	9.3	6.5	1.9	0.70	0.20
Taipivai	Nuku Hiva	*[45]*	2.5	6.0	1.0	2.40	0.40
Taiohae east	Nuku Hiva	*[49]*	10.1	6.5	1.2	0.64	0.12
Taiohae west	Nuku Hiva	*[51]*	5.2	5.5	0.7	1.06	0.13
Pitcairn Island							
Bounty Bay	Pitcairn	*[65]*	5.0	3.0	1.2	0.60	0.24
Easter Island							
Hanga Roa	Rapa Nui	*[54]*	8.6	3.5	1.6	0.41	0.19
Juan Fernández Islands							
S. Juan Batista	Robinson Crusoe	*[52]*	2.7	2.5	0.35	0.93	0.13

Using this definition, we find an average residual $\bar{r} = -0.09 \pm 0.14$ logarithmic unit for our data set of 27 locations. In other words, our simulated amplitudes are on the average 81% of the measured run-up values with a scatter corresponding to a multiplicative or divisive factor ($*/$) of 1.44. Given the potential influence of unknown details in bathymetry and topography, we conclude that the earthquake source satisfactorily explains the distribution of run-up in the far-field islands.

By contrast, the dipolar model leads to $\bar{r} = -0.62 \pm 0.19$; in other words, amplitudes simulated using the landslide source are on the average only 24% $^*/1.55$ of the measured run-up. Note in particular that the standard deviations of the two populations of residuals are very comparable, and as such, the two data sets are well separated and essentially incompatible. Furthermore, the ratio (3.4 on the average) between the simulated run-ups of the landslide and earthquake sources separates, at most stations, a relatively benign tsunami from a much more damaging one. In particular, at the 19 sites in the Marquesas Islands, the average run-up of the former (1.4 m) would result in only moderate damage (at most capsizing of small boats and some limited beach erosion), while the average run-up of 5 m expected from the latter explains flooding and destruction of houses hundreds of metres inland as reported by eyewitnesses, and matches the average measured value of 5.9 m. On this basis, we conclude that the surveyed data set is well explained by the dislocation source based on López & Okal's (2006) seismological model, but reject the landslide source as the generator of the far-field tsunami. Note in particular that because the landslide source satisfactorily explains the tsunami in the near field, it is not possible to simply scale it upwards to match the far-field data set.

As discussed above, the low values of run-up measured in the Austral Islands reflect the presence of coral reefs and shallow lagoons, particularly well developed at Tubuai and Raivavae. These are well matched by the simulated values, even though the azimuths of the great circle paths at the epicentre are exactly in the direction of the directivity lobe of the dislocation source, as computed using an extension of Ben-Menahem & Rosenman's (1972) formalism to the case of a bilateral rupture and plotted on Fig. 1 for a tsunami wave with a period of 1000 s. By contrast, a low run-up value was surveyed by Okal *et al.* (2002) at Juan Fernández (2.7 m), and also well simulated using the dislocation source (2.5 m). Robinson Crusoe Island is a young volcanic structure (Gripp & Gordon 2002) at high latitude (34°S), precluding the existence of even a submerged coral reef; the low run-up value is thus a clear illustration of the destructive interference due to the finiteness of the source at an azimuth of 50° from the lobe of directivity (Fig. 1). As discussed by Okal (2003), strong, narrow lobes of directivity in the far-field cannot be generated by landslide sources whose physical velocities remain slower than the phase velocity of a tsunami on the high seas,

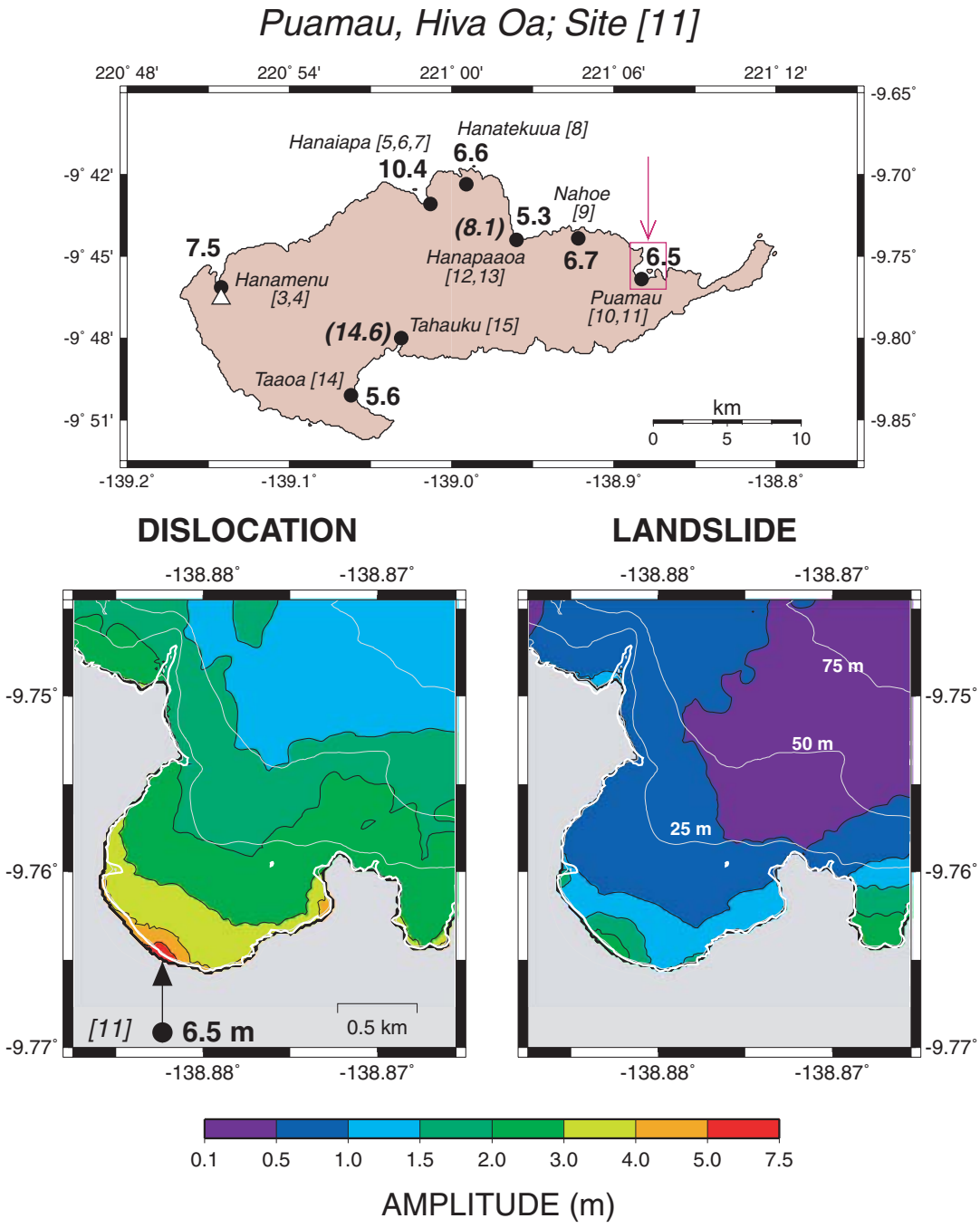

Figure 5. Simulation results at Puamau, Hiva Oa (Site *[11]*). The site under study is identified by the red box and arrow on the map on top, adapted from Okal *et al.* (2002). The maximum amplitude of the wave over a 2-hr window following the arrival of the tsunami is contoured inside the bay and on initially dry land for the dislocation model (left) and the landslide one (right). The white contours represent the unperturbed shore line (bold) and the 25, 50 and 75 m isobaths.

resulting in destructive interference in all azimuths. Thus, the co-existence in the Central and South Pacific and at neighbouring azimuths of high tsunami amplitudes (in the Marquesas) and low ones (at Juan Fernández) is well explained and modelled by a dislocation source, but irreconcilable with a landslide one.

In a number of instances, Table 1 and Fig. 6 feature a less than satisfactory fit between simulated and measured values of run-up. In particular, at Site *[45]* (Taipivai, Nuku Hiva), the simulated run-up is 2.4 times greater than observed. This probably reflects the extreme horizontal inundation reaching more than 500 m at that location (and 1250 m in the nearby riverbed) in that very flat valley (Okal *et al.* 2002); in this context, our simulations which neglect the effect of friction must be overestimating run-up at the site. By contrast, at Easter Island (Site *[54]*) and Hanaiapa, Hiva Oa (Site *[7]*), run-up is clearly undersimulated, a probable result of the steep topographic gradients along the path of inundation.

(2) *Virtual tidal gauge records.* On Fig. 7, we examine the case of the response of Taiohae Bay, on the Southern shore of Nuku Hiva. We consider two virtual gauges located over the isobaths 50 and 7 m, respectively, whose time-series are plotted on the top frames. The blue lines represent simulations using the landslide source, and

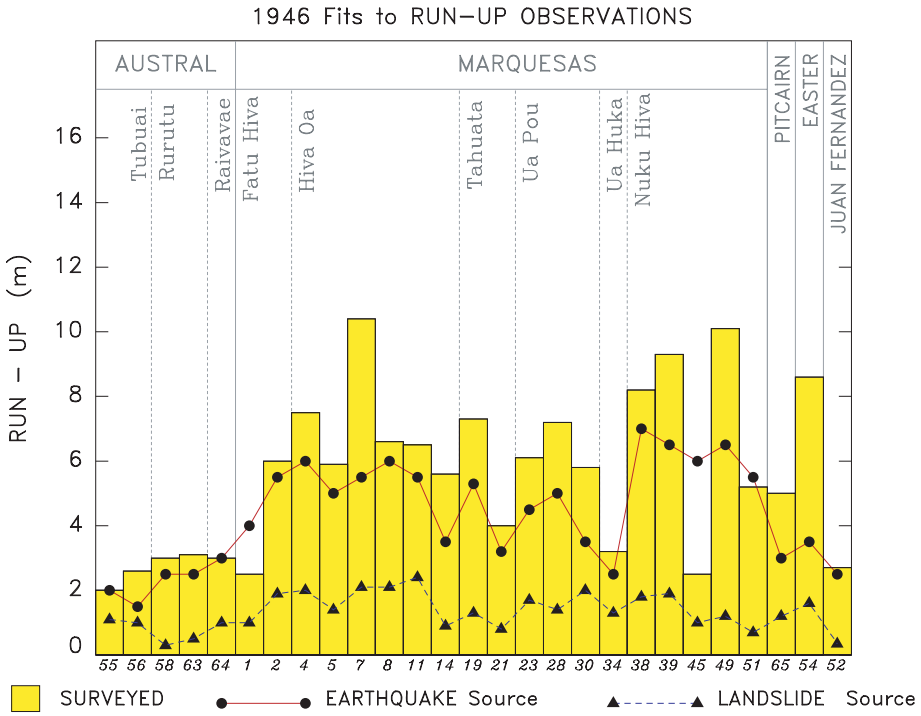

Figure 6. Summary of simulation results for the 27 sites studied. At each location, the full bar represents the measured run-up, the dots linked by the solid line the values simulated from the dislocation source, and the triangles linked by the dashed line those using the dipolar source. The stations are arranged in the same order as in Table 1, with reference numbers listed under each bar.

the red ones using the dislocation source. Note that the dislocation source produces a wave of much larger amplitude at the entrance of the bay ($h = 50$ m), which is further amplified by a greater factor than in the case of the landslide source, reaching a peak-to-peak amplitude of 8 m for $h = 7$ m, as compared to 0.5 m for the dipolar source. This property is further investigated by considering the spectra of the virtual gauge records in the bottom frames of Fig. 7. At the entrance of the bay (dark traces), the dislocation wavefield is peaked around 0.9 mHz (corresponding to a period of 19 mn), while the landslide spectrum is essentially white between 0.8 and 5 mHz (at considerably smaller spectral amplitudes). At the second gauge ($h = 7$ m), the low-frequency components around 1 mHz are amplified considerably (by a factor of 3), while those at 3 mHz remain unchanged. This expresses an obvious resonance of the bay around 0.9–1 mHz, which explains the large amplitudes reported at Taiohae (up to 10.1 m on the east side of the bay). Note that only the wavefield produced by the dislocation is capable of a strong resonance since it is already strongly peaked at the appropriate frequency as it enters the bay, while the landslide wavefield, being broader and generally of higher frequency, is not amplified in the same fashion. This constitutes an additional argument in favour of the generation of the far-field tsunami by the seismic dislocation.

6 CONCLUSION

On the basis of the hydrodynamic simulation of run-up values of the 1946 Aleutian tsunami at 27 transpacific locations, we show that the earthquake dislocation source recently proposed by López & Okal (2006) satisfactorily explains the principal properties of the data set of values measured from the testimony of elderly witnesses, as compiled by Okal *et al.* (2002) and updated as part of the present study. Namely, the amplitude of the simulated run-up is on the average 81% of that measured, and we reproduce the rapid azimuthal decay of the amplitude of the wave when moving laterally outside the lobe of directivity due to source finiteness, as evidenced at Juan Fernández Islands, in accordance with Ben-Menahem & Rosenman's (1972) model. We note that a largely similar dislocation source was also used by Titov & González (2003) to successfully model the inundation at Hilo, Hawaii during the 1946 Aleutian tsunami.

On the other hand, the dipolar source based on the model of a large underwater landslide, which Okal *et al.* (2003) had used to explain the exceptional near-field run-up at Scotch Cap, fails to match our data set of observed values in the far field, producing minimal amplitudes which would generally not have caused the kind of observable damage widely reported, especially in the Marquesas Islands. It also generates wavefields with a higher-frequency spectrum, all these observations being in line with general scaling concepts, as developed for example by Okal (2003) and Okal & Synolakis (2004).

The picture emerging from the combination of the present study and the previous work of López & Okal (2006) is that of a remarkably slow, but very large, earthquake which triggered a significant landslide along the continental slope to the South of Davidson Bank. As discussed by these authors, the landslide is expected to be silent seismically, especially in the presence of a large, slow, earthquake. Nevertheless, it is required by the exceptional amplitude and concentration of the tsunami in the near field, which cannot be ascribed to a dislocation source in the framework of seismic scaling laws, as discussed by Okal & Synolakis (2004). Because of its spatial concentration, dramatized on Fig. 3, the landslide generates a wavefield of shorter wavelengths, which fails to propagate efficiently in the far field. Thus the contribution of the landslide to the far-field tsunami is negligible, and the latter is well explained by the earthquake dislocation, as would be expected from its mere size, at 8.5×10^{28} dyn-cm, one of the ten largest earthquakes ever recorded.

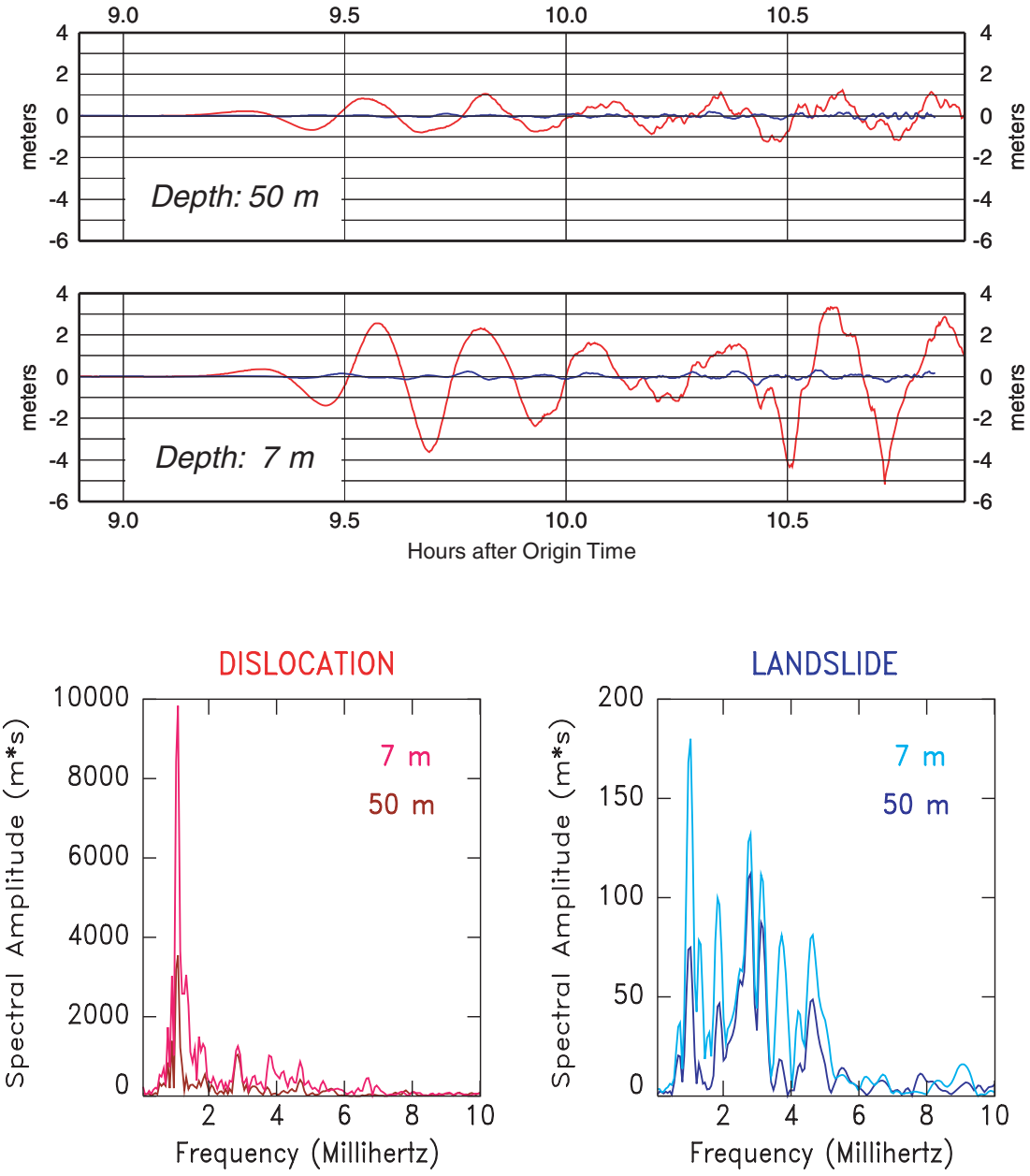

Figure 7. (Top) Maregrams simulated at virtual gauges located on the 50 and 7 m isobaths in Taiohae Bay (Nuku Hiva; Marquesas). The red lines use the dislocation source and the blue ones the landslide source. Note the clear difference in period and amplification by the bay. (Bottom) Spectral amplitude of the virtual maregrams simulated from the dislocation (left) and landslide (right) sources. For each source, the 50 m gauge is plotted in darker color and the 7 m one as the brighter line on the same scale. Note the much reduced amplitude for the landslide source even at the entrance of the bay, and the selective amplification of the bay around 0.9 mHz.

ACKNOWLEDGMENTS

We thank Costas Synolakis for discussion, Guilhem Barruol and Malcolm McCullogh for the data collected at Raivavae and Pitcairn, respectively, and Yoann Cano for help in the field at Tubuai and Rurutu. This study was supported by the National Science Foundation, under Grant CMS-03-01054 to EAO, and by Commissariat à l'Energie Atomique. The comments of two anonymous reviewers helped improve the final version of the manuscript. Some figures were drafted using the GMT software package (Wessel & Smith 1991).

REFERENCES

Ben-Menahem, A. & Rosenman, M., 1972. Amplitude patterns of tsunami waves from submarine earthquakes, *J. Geophys. Res.,* **77,** 3097–3128.

Chauvel, C., McDonough, W., Guille, G., Maury, R. & Duncan, R., 1997. Contrasting old and young volcanism in Rurutu Island, Austral chain, *Chem. Geol.,* **139,** 125–143.

Courant, R., Friedrichs, K. & Lewy, H., 1928. Über die partiellen Differenzengleichungen der mathematischen Physik, *Mathematische Annalen,* **100,** 32–74.

Duncan, R.A., Mcdougall, I., Carter, R.M. & Coombs, D.S., 1974. Pitcairn Island — another Pacific hotspot, *Nature,* **251,** 679–682.

Fryer, G.J., Watts, P. & Pratson, L.F., 2004. Source of the great tsunami of 1 April 1946: a landslide in the upper Aleutian forearc, *Mar. Geol.,* **203,** 201–218.

Fuchs, V., 1982. *Of ice and men: The history of the British Antarctic Survey, 1943–73*. A. Nelson, Oswestry, 383 pp.

Fukao, Y., 1979. Tsunami earthquakes and subduction processes near deep-sea trenches, *J. Geophys. Res.,* **84,** 2303–2314.

Gripp, A.E. & Gordon, R.G., 2002. Young tracks of hotspots and current plate velocities, *Geophys. J. Intl.,* **150,** 321–361.

Guibourg, S., Heinrich, P. & Roche, R., 1997. Numerical modeling of the 1995 Chilean tsunami. Impact on French Polynesia, *Geophys. Res. Letts.,* **24,** 775–778.

Gutenberg, B. & Richter, C.F., 1954. *Seismicity of the Earth and Associated Phenomena,* Princeton Univ. Press, Princeton, NJ, 310 pp.

Hébert, H., Heinrich, P., Schindelé, F. & Piatanesi, A., 2001. Far-field simulation of tsunami propagation in the Pacific ocean; impact on the Marquesas Islands (French Polynesia), *J. Geophys. Res.,* **106,** 9161–9177.

Heinrich, P., Piatanesi, A., Okal, E.A. & Hébert, H., 2000. Near-field modeling of the July 17, 1998 tsunami in Papua New Guinea, *Geophys. Res. Letts.,* **27,** 3037–3040.

Johnson, J.M. & Satake, K., 1997. Estimation of seismic moment and slip distribution of the April 1, 1946, Aleutian tsunami earthquake, *J. Geophys. Res.,* **102,** 11765–11774.

Kanamori, H., 1972. Mechanism of Tsunami Earthquakes, *Phys. Earth Planet. Inter.,* **6,** 346–359.

Kanamori, H., 1985. Non-double-couple seismic source, *Proc. XXIIIrd Gen. Assemb. Intl. Assoc. Seismol. Phys. Earth Inter.,* p. 425, Tokyo [abstract].

López, A.M. & Okal, E.A., 2006. A seismological reassessment of the source of the 1946 Aleutian "tsunami" earthquake, *Geophys. J. Intl.,* **165,** 835–849.

MacDonald, G.A., Shepard, F.P. & Cox, D.C., 1947. The tsunami of April 1, 1946 in the Hawaiian Islands, *Pacif. Sci.,* **1,** 21–37.

Mansinha, L. & Smylie, D.E., 1971. The displacement fields of inclined faults, *Bull. Seismol. Soc. Amer.,* **61,** 1433–1440.

Okal, E.A., 2003. Normal modes energetics for far-field tsunamis generated by dislocations and landslides, *Pure. Appl. Geophys.,* **160,** 2189–2221.

Okal, E.A. & Synolakis, C.E., 2004. Source discriminants for near-field tsunamis, *Geophys. J. Intl.,* **158,** 899–912.

Okal, E.A. *et al.,* 2002. A field survey of the 1946 Aleutian tsunami in the far field, *Seismol. Res. Letts.,* **73,** 490–503.

Okal, E.A., Plafker, G., Synolakis, C.E. & Borrero, J.C., 2003. Near-field survey of the 1946 Aleutian tsunami on Unimak and Sanak Islands, *Bull. Seismol. Soc. Amer.,* **93,** 1226–1234.

Pelayo, A., 1990. Earthquake source parameter inversion using body and surface waves: applications to tsunami earthquakes and to Scotia Sea seismotectonics, *Ph.D. thesis,* Washington Univ., St. Louis.

Sanford, H.B., 1946. *Log of Coast Guard unit number 368, Scotch Cap DF Station, relating to the Scotch Cap light station tragedy*. U.S. Coast Guard, Washington, D.C., 11 pp.

Smith, W.H.F. & Sandwell, D.T., 1997. Global seafloor topography from satellite altimetry and ship depth soundings, *Science,* **277,** 957–1962.

Synolakis, C.E., J.-P. Bardet, J.C. Borrero, H.L. Davies, E.A. Okal, E.A. Silver, S. Sweet & D.R. Tappin, 2002. The slump origin of the 1998 Papua New Guinea tsunami, *Proc. Roy. Soc. (London), Ser. A,* **458,** 763–789.

Tanioka, Y. & Seno, T., 2001. Detailed analysis of tsunami waveforms generated by the 1946 Aleutian tsunami earthquake, *Nat. Haz. Earth Syst. Sci.,* **1,** 171–175.

Titov, V.V. & González, F.I., 2003. Modeling solutions for short-term inundation forecasting for tsunamis, in: *Submarine Landslides and Tsunamis,* eds. A.C. Yalçıner, E.N. Pelinovsky, E.A. Okal & C.E. Synolakis, NAT O Sci. Ser., pp. 277–284, Kluwer, Amsterdam.

Wessel, P. & Smith, W.H.F., 1991. Free software helps map and display data, *Eos, Trans. Amer. Geophys. Un.,* **72,** 441 and 445–446.